

A study of cooperative breathing-mode in molecular chains

Ravindra Pankaj¹ and Sudhakar Yarlagadda^{1,2}

¹ TCMP Div., Saha Institute of Nuclear Physics, Kolkata, India and

² Cavendish Lab, Univ. of Cambridge, Cambridge, UK

(Dated: November 16, 2018)

Using a controlled analytic non-perturbative treatment, that accounts for the quantum nature of the phonons, we derive a model that generically describes cooperative breathing-mode at strong electron-phonon interaction in one-band one-dimensional systems. The effective model involves a *next-nearest-neighbor* hopping (that dominates over the nearest-neighbor hopping at strong coupling) and a nearest-neighbor repulsion that is significantly enhanced due to incompatibility of neighboring dilations/compressions. At non-half filling, upon tuning the electron-phonon coupling, the system undergoes a period-doubling second-order quantum phase transition from a Luttinger liquid to a *conducting commensurate* charge-density-wave state: a phenomenon absent in both the Holstein model and the t-V model. Using fidelity to study the nature of the quantum phase transition, we find that the fidelity susceptibility shows a superextensive power law divergence as well as a remarkable scaling behavior: both together establish a second-order transition.

PACS numbers: 71.38.-k, 71.45.Lr, 71.38.Ht, 75.47.Lx

I. INTRODUCTION

Perovskite materials are quite ubiquitous and exhibit a variety of interesting and intriguing phenomena such as superconductivity or charge ordering (or their co-existence), colossal magnetoresistance, ferroelectricity, spin-dependent-transport, and the interplay among magnetic, structural, and transport properties^{1–3}. Many oxides, that have the formula ABO_3 , assume a perovskite structure where two adjacent BO_6 octahedra share an oxygen which leads to cooperative octahedral distortions. Simple systems that manifest such cooperative electron-phonon phenomena are the barium bismuthates ($BaBiO_3$). Here, only the 6s electrons are involved in transport and these electrons produce only a single normal mode distortion, namely, the breathing-mode. In pure $BaBiO_3$, the BO_6 octahedra alternately dilate and contract with $Bi - O$ bonds of adjacent octahedra differing by about 10% which is indicative of strong electron-phonon interaction (EPI)¹. Thus the relevant physics is dominated by a one-band three-dimensional cooperative breathing-mode (CBM).

There is also compelling evidence of strong EPI in manganites (from extended X-ray absorption fine structure⁴ and pulsed neutron diffraction⁵ measurements) and in cuprates (through angle-resolved photoemission spectroscopy⁶).

In copper oxides, as pointed out in Refs. 7 and 8, the dynamics of the Zhang-Rice singlet⁹ can be described by a one-band system with orbitals centered on copper sites. Furthermore, the onsite energy is modulated by the movement of oxygen closer or further from the neighboring copper ion. Thus the breathing-mode is relevant to describe the linear modulation of the onsite energy. Consequently the copper-oxide planes represent a one-band two-dimensional CBM system.

In the context of the two-band Jahn-Teller manganite systems as well, when C-type antiferromagnetism man-

ifests [as in $La_{1-x}Sr_xMnO_3$ for $0.65 \leq x \leq 0.9^{10}$], the d_{z^2} orbitals participate in the C-chain ordering. A ferromagnetic C-chain can be looked upon as a one-band (i.e., d_{z^2} orbital band) and one-dimensional (1D) CBM system that is however Jahn-Teller coupled to neighboring C-chains whose spin alignment is antiparallel.

Understanding the CBM phenomena, in systems such as the bismuthates, the cuprates, and the manganites is still an open question. The main purpose of this paper is to study the CBM physics in the simpler case of a one-band 1D system by taking account of the *quantum phonons* [see Fig. 1(b)]. In fact, a controlled analytic treatment of the many-polaron effects produced by quantum phonons in a one-band 1D Holstein model [see Fig. 1(a)]¹¹ (which is a simpler non-cooperative EPI system) has been reported not long ago^{12,13}. However, definite progress has been made in numerically treating the Holstein model at half-filling (by employing a variety of techniques)^{14–19} and, to a limited extent, away from half-filling²⁰.

Owing to its cooperative nature, the EPI leads to non-local distortion effects which can change the very nature of long range order. While a weak interaction is amenable to a Migdal-type of perturbative treatment, the strong interaction (even for a one-band system) necessitates a non-perturbative approach¹². As a step towards modeling CBM distortions in real systems (such as the bismuthates, the cuprates, and the manganites), the present work builds up on our previous work on the Holstein model¹² to obtain the effective Hamiltonian for a one-band 1D CBM system^{21–23}. Upon inclusion of cooperative effects in the strong EPI, we show that the system changes its dominant transport mechanism from one of nearest-neighbor (NN) hopping to that of next-nearest-neighbor (NNN) hopping while the effective NN electron-electron interaction becomes significantly more repulsive due to incompatibility of NN breathing mode distortions. Away from half-filling in rings with even number of sites

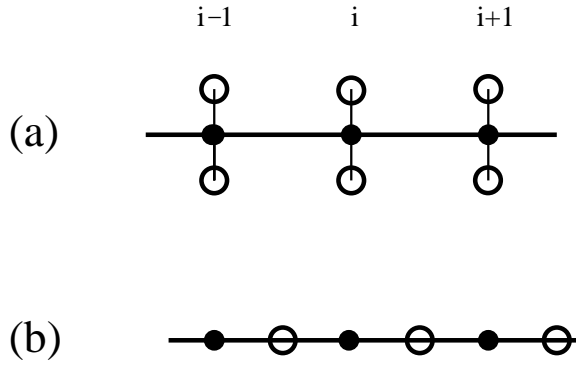


FIG. 1. Molecular chains with d_{z2} orbital hopping sites (filled circles) and oxygen sites (empty circles) in (a) Holstein model, (b) one-band CBM system.

(while the Holstein system without cooperative effects remains a Luttinger liquid at all interaction strengths), our model (at strong interaction), produces a commensurate charge-density-wave (CDW) state which is surprisingly conducting and whose period is independent of density. Furthermore, using scaling of the fidelity susceptibility (FS), we demonstrate that the CDW transition is a second-order quantum phase transition (QPT).

The paper is organized as follows. We derive an effective polaronic Hamiltonian starting from a CBM model in Sec. II. Next, we present the relevant formulae for the density-density correlation function and the structure factor in Sec. III. We then analyze the strong-coupling limiting case of our CBM model in Sec. IV. The nature of the QPT and the long range order in our CBM model are discussed in Sec. V. Finally, we close in Sec. VI with our conclusions.

II. EFFECTIVE POLARONIC HAMILTONIAN

To bring out the essential physics, we begin with a 1D model of spinless electrons hopping in a one-band system of d_{z2} orbitals which are coupled to the oxygens in between, via CBM as shown in Fig. 1(b)⁷. The Hamiltonian is expressed as $H = H_t + H_{ep} + H_l$ where the hopping term H_t , using standard notation, is given by

$$H_t = -t \sum_j (c_j^\dagger c_{j+1} + \text{H.c.}), \quad (1)$$

with c_j (c_j^\dagger) being the destruction (creation) operator of an electron in a d_{z2}^j orbital (at site j). The EPI term H_{ep} is expressed as

$$H_{ep} = -g\omega_0 \sqrt{2M\omega_0} \sum_j n_j q_j, \quad (2)$$

where g is the electron-phonon coupling (EPC), $n_i = c_i^\dagger c_i$, $q_i = u_i - u_{i-1}$ represents the expansion of the oxygens around the d_{z2}^i orbital, and the right-hand-side

(RHS) oxygen displacement $u_i = (a_i^\dagger + a_i)/\sqrt{2M\omega_0}$. Furthermore, the lattice term H_l representing simple harmonic oscillators is of the form

$$H_l = \frac{K}{2} \sum_j u_j^2 + \frac{1}{2M} \sum_j p_j^2 = \omega_0 \sum_j a_j^\dagger a_j. \quad (3)$$

The main difference between the Holstein model and the above cooperative Hamiltonian is that in the Holstein model electrons at different sites are coupled to different on-site molecular distortions whereas in the present system the electrons on adjacent sites are coupled to the displacement of the same in-between oxygen. Thus in our system, to produce an effective polaronic Hamiltonian, we need to devise a modification of the usual Lang-Firsov transformation²⁴ so as to take into account the cooperative nature of the distortions. To meet this end, we used the following canonical transformation $\tilde{H} = \exp(S)H \exp(-S)$ where S now contains the *difference in densities on adjacent sites*

$$S = g \sum_j (a_j - a_j^\dagger)(n_j - n_{j+1}). \quad (4)$$

Then, one obtains $\tilde{H} = H_0 + H_1$ where

$$H_0 = \omega_0 \sum_j a_j^\dagger a_j - 2g^2 \omega_0 \sum_j n_j + 2g^2 \omega_0 \sum_j n_j n_{j+1} - te^{-3g^2} \sum_j (c_j^\dagger c_{j+1} + \text{H.c.}), \quad (5)$$

and

$$H_1 = \sum_j H_{1j} = -te^{-3g^2} \sum_j [c_j^\dagger c_{j+1} \{\mathcal{T}_-^{j\dagger} \mathcal{T}_+^j - 1\} + \text{H.c.}],$$

with $\mathcal{T}_\pm^j = \exp[\pm g(2a_j - a_{j-1} - a_{j+1})]$. On account of the cooperative nature of the EPI we obtain an additional term $2g^2 \omega_0 \sum_j n_j n_{j+1}$ involving NN repulsion in H_0 and the perturbation H_1 now involves phonons at three sites as opposed to phonons at only two sites as in the non-cooperative case. We consider the case $t \exp[-3g^2] \ll \omega_0$ and perform second-order perturbation theory similar to that in Refs. 12 and 25. The eigenstates of H_0 relevant for perturbation theory are $|n, m\rangle \equiv |n\rangle_{el} \otimes |m\rangle_{ph}$ where NN occupied electronic states are projected out and $|0, 0\rangle$ is the ground state (GS) with no phonons. The corresponding eigenenergies are $E_{n,m} = E_n^{el} + E_m^{ph}$. The treatment to perform second-order perturbation theory is an extension of the method followed in Refs. 12 and 25 and yields the following effective Hamiltonian for polarons:

$$H^{(2)} = \sum_{i,j} \sum_m \frac{\langle 0|_{ph} H_{1i} |m\rangle_{ph} \langle m|_{ph} H_{1j} |0\rangle_{ph}}{E_0^{ph} - E_m^{ph}}. \quad (6)$$

Here (as shown by using Schrieffer-Wolff transformation in appendix A of Refs. 25 and 26), it must be mentioned that, when $t \exp[-3g^2] \ll \omega_0$, $H_0 + H^{(2)}$ represents the exact Hamiltonian up to second-order in perturbation

(even for finite anti-adiabatic values $t/\omega_0 \lesssim 1$); the small parameter $[t/(g\omega_0)]$ of the perturbation will be derived below. In the above equation (6), unlike in Ref. 12, the term H_j produces phonons at sites j , $j-1$, and $j+1$. Hence, we get non-zero contributions only when the index $i = j-2$, $j-1$, j , $j+1$, or $j+2$. Then after some tedious algebra one obtains

$$\begin{aligned} -H^{(2)} \frac{\omega_0}{t^2 e^{-6g^2}} = & \sum_j \{ [n_j(1-n_{j+1}) + (1-n_j)n_{j+1}] \\ & [F_3(4,1,1) + 2F_2(4,1) + F_1(4) + 2F_1(1) + F_2(1,1)] \\ & + [c_{j-1}^\dagger(1-2n_j)c_{j+1} + \text{H.c.}] [2F_1(2) + F_2(2,2)] \\ & + 2[c_{j-2}^\dagger c_{j-1} c_{j+1}^\dagger c_j + \text{H.c.}] F_1(1) \\ & + 2[c_{j-1}^\dagger c_{j-2} c_{j+1}^\dagger c_j + \text{H.c.}] F_1(-1) \} , \end{aligned} \quad (7)$$

where

$$F_n(\alpha_1, \dots, \alpha_n) \equiv \sum_{m_1=1}^{\infty} \dots \sum_{m_n=1}^{\infty} \frac{(\alpha_1 g^2)^{m_1} \dots (\alpha_n g^2)^{m_n}}{m_1! \dots m_n! (m_1 + \dots + m_n)},$$

which for large values of g^2 becomes $F_n \approx \exp(g^2 \sum_{i=1}^n \alpha_i) / (g^2 \sum_{i=1}^n \alpha_i)$ for $\sum_{i=1}^n \alpha_i \geq 1$. In the above Eq. (7), the last two terms are a direct consequence of the cooperative nature of the EPI and are negligible for large g^2 . More importantly, the relative importance of the various coefficients is noticeably different from the case where no cooperative effect exists (as explained below). For large g^2 , the effective polaronic Hamiltonian simplifies to be:

$$\begin{aligned} H_{eff}^C = & - \left[2g^2\omega_0 + \frac{t^2}{3g^2\omega_0} \right] \sum_j n_{j+1}(1-n_j) \\ & - te^{-3g^2} \sum_j (c_j^\dagger c_{j+1} + \text{H.c.}) \\ & - \frac{t^2 e^{-2g^2}}{4g^2\omega_0} \sum_j [c_{j-1}^\dagger(1-2n_j)c_{j+1} + \text{H.c.}] . \end{aligned} \quad (8)$$

Notice that the coefficient of the NN hopping is significantly smaller than the coefficient of the NNN hopping for large g^2 and not-too-small t/ω_0 ! This is a *key feature resulting from cooperative effects*. The above effective Hamiltonian H_{eff} for the case where there is no cooperative EPI [i.e., $H_{ep} = -\sqrt{2}g\omega_0 \sum_i n_i(a_i^\dagger + a_i)$] [see Ref. 12 and Fig. 1(a)]:

$$\begin{aligned} H_{eff} = & -2g^2\omega_0 \sum_j n_j - \frac{t^2}{2g^2\omega_0} \sum_j n_{j+1}(1-n_j) \\ & - te^{-2g^2} \sum_j (c_j^\dagger c_{j+1} + \text{H.c.}) \\ & - \frac{t^2 e^{-2g^2}}{2g^2\omega_0} \sum_j [c_{j-1}^\dagger(1-2n_j)c_{j+1} + \text{H.c.}] . \end{aligned} \quad (9)$$

We now provide an explanation of the above results. In Eq. (9), the coefficient of the $\sum_j n_{j+1}(1-n_j)$ term can be understood as resulting from a hopping process where an electron at site $j+1$ hops to a neighboring site j and back, but the lattice has no time to distort (relax) *locally* at site j ($j+1$) and thus yields the second-order perturbation energy $-t^2/(\text{energy change})$ (see Fig. 2 of Ref. 25). On the other hand, the coefficient of $\sum_j [c_{j-1}^\dagger(1-2n_j)c_{j+1} + \text{H.c.}]$ results when, in the intermediate state, site j does not distort/relax during hopping and thus yields $t \exp[-2g^2] \times \frac{t}{2g^2\omega_0}$ where $t \exp[-2g^2]$ is due to time $\left(\frac{\hbar}{te^{-2g^2}}\right)$ taken to distort the site $j+1$ (see Fig. 2 of Ref. 25). In the above non-cooperative case, the NN hopping dominates over the NNN hopping in the small polaron limit.

Using the above logic we see that the higher order terms in perturbation theory, for both cooperative and non-cooperative cases, are dominated by the process where an electron hops back and forth between the same two sites. The dominant term to k th order is approximately given for even k by

$$\omega_0 \left[\frac{t}{g\omega_0} \right]^k \sum_j n_{j+1}(1-n_j), \quad (10)$$

while for odd k by

$$te^{-\gamma g^2} \left[\frac{t}{g\omega_0} \right]^{k-1} \sum_j (c_j^\dagger c_{j+1} + \text{H.c.}), \quad (11)$$

where γ is 2 for the non-cooperative case and 3 for the cooperative one. Since each term in the perturbation theory should be smaller than ω_0 , we see that the small parameter in our perturbation theory is $t/(g\omega_0)^{13}$.

Here, a few observations are in order. Firstly, the cooperative effects, unlike in the Holstein model's case, raise the potential of the site next to an occupied site and thus make it unfavorable for hopping. Consequently, in Eq. (8) as compared to Eq. (9), the exponent is larger for the NN hopping and also the denominators of the coefficients are similarly larger for the hopping-generated NN interaction and for the NNN hopping. Next, Lau *et al.*⁷ obtain the same energy expression for a *single polaron* as that given by Eq. (8) (when $n_j = 0$). Additionally, in Ref. 27, the authors explain the ferromagnetic insulating behavior in low-doped manganites by using the non-cooperative hopping-generated NN interaction [i.e., second term on RHS of Eq. (9)] after modifying the hopping term for double-exchange effects. From Eq. (8), we see that cooperative phenomenon must be taken into account as it reduces the ferromagnetism generating interaction strength by a factor of 1.5. Lastly, the authors of Refs. 28 and 29 study the formation of bipolarons using Fröhlich polarons with spin degrees of freedom; although they use a Lang-Firsov transformation followed by a Schrieffer-Wolff transformation (which is similar to our type of perturbation theory), they nevertheless do

not consider the dominant NNN hopping effects which are central to our treatment.

In the next few sections, we will analyze the effective polaronic Hamiltonian given by Eq. (8) and show that there is a period-doubling QPT from a Luttinger liquid to a conducting CDW when the coupling g increases at fixed adiabaticity t/ω_0 ; the transition is a consequence of enhanced NNN hopping and pronounced NN repulsion. We employ a modified Lanczos algorithm³⁰ [and use antiperiodic (periodic) boundary conditions for even (odd) number of fermions] to study the QPT in the system. In all our numerical calculations involving the effective polaronic Hamiltonian, we used the series $F_n(\alpha_1, \dots, \alpha_n)$ given in Eq. (7) and not the approximate coefficients in Eq. (8).

III. DENSITY-DENSITY CORRELATION FUNCTION AND STRUCTURE FACTOR

In this section, to characterize correlations and analyze QPT, we present the relevant formulae for the density-density correlation function and the structure factor. The two-point correlation function for density fluctuations of electrons at a distance l apart is given by

$$W(l) = \frac{4}{N} \sum_j [\langle n_j n_{j+l} \rangle - \langle n_j \rangle \langle n_{j+l} \rangle], \quad (12)$$

with filling-fraction (FF) $\langle n_j \rangle = \frac{N_p}{N}$ where N is the total number of sites and N_p is the total number of electrons in the system. Then the structure factor, which is the Fourier transform of $W(l)$, is given by

$$S(k) = \sum_l e^{ikl} W(l), \quad (13)$$

where wavevector $k = \frac{2n\pi}{N}$ with $n=1, 2, \dots, N$. Now, we observe that

$$S(\pi) = \left(\sum_{l_{\text{even}}} - \sum_{l_{\text{odd}}} \right) W(l),$$

with

$$\sum_{l_{\text{even}}} W(l) = \frac{2\langle (\hat{N}_e - \hat{N}_o)^2 \rangle}{N},$$

and

$$\sum_{l_{\text{odd}}} W(l) = -\frac{2\langle (\hat{N}_e - \hat{N}_o)^2 \rangle}{N},$$

where $\hat{N}_e = \sum_{j_{\text{even}}} n_j$ ($\hat{N}_o = \sum_{j_{\text{odd}}} n_j$) is the number operator which gives the total number of electrons at even (odd) sites. Hence, we obtain the simple expression

$$S(\pi) = \frac{4\langle (\hat{N}_e - \hat{N}_o)^2 \rangle}{N}. \quad (14)$$

We will now analyze the situation where only one sub-lattice is occupied and obtain some exact results. When we consider odd values of l , we note that

$$\langle n_j n_{j+l} \rangle = 0.$$

Hence, from Eq. (12) we get

$$W(l_{\text{odd}}) = -\frac{4N_p^2}{N^2}. \quad (15)$$

Next, we observe that the GS becomes an eigenstate of the operators \hat{N}_e and \hat{N}_o with the eigenvalues N_p (0) and 0 (N_p) respectively if the even-site (odd-site) sub-lattice is occupied. Consequently, we get

$$[S(\pi)] = [S(\pi)]_{\text{max}} = \frac{4N_p^2}{N}, \quad (16)$$

where $[S(\pi)]_{\text{max}}$ is the maximum value that $S(\pi)$ can attain.

To analyze the QPTs, we can treat the rescaled value of $S(\pi)$ as the order parameter $S^*(\pi)$ defined as follows:

$$S^*(\pi) = \frac{S(\pi) - [S(\pi)]_{\text{min}}}{[S(\pi)]_{\text{max}} - [S(\pi)]_{\text{min}}}, \quad (17)$$

where $[S(\pi)]_{\text{min}}$ is the minimum value of $S(\pi)$; consequently, $S^*(\pi)$ varies from 0 to 1 during the phase transition.

In the next section, we will study the limiting case of large EPC values where the NNN hopping is the only relevant transport mechanism in the CBM model leading to the t_2 -V model [see Eq. (19)].

IV. ANALYSIS OF THE t_2 -V MODEL – A LIMITING CASE OF THE CBM MODEL

The effective Hamiltonian for the CBM model contains three terms, namely, NN hopping, NNN hopping, and NN repulsion [as can be seen from Eq. (8)]. There are two possible extreme cases of the CBM model corresponding to small and large values of the EPC g . For small values of g (~ 1), NN hopping dominates over NNN hopping; consequently, Eq. (8) reduces to

$$H_{tV} \equiv -t \sum_j (c_j^\dagger c_{j+1} + \text{H.c.}) + V \sum_j n_j n_{j+1}, \quad (18)$$

which is the well studied t-V model^{30,31} with $t/V \ll 1$ at the small values of g (~ 1) considered.

On the other hand, for large values of g , NNN hopping dominates over NN hopping and Eq. (8) can be simplified to

$$H_{t_2V} \equiv -t_2 \sum_j (c_{j-1}^\dagger (1 - 2n_j) c_{j+1} + \text{H.c.}) + V \sum_j n_j n_{j+1}, \quad (19)$$

which we shall call as the t_2 -V model; here, since EPC is large (i.e., $g \gtrsim 3$), $t_2/V \ll 1$. However, owing to the novelty of the model, we shall study it [i.e., Eq. (19)] for arbitrary values of t_2/V in rings with even number of sites. Next, for $t_2/V \ll 1$, we note that the system always has alternate sites (i.e., one sub-lattice) occupied for less than half-filling and above half-filling the other sub-lattice gets filled. This can be explained, for less than half-filling, as follows. At large repulsion, we shall compare the energy for the following two situations:

1. When there are $m_A > 0$ ($m_B > 0$) electrons in sub-lattice A (B).
2. When all the $m_A + m_B = N_p$ electrons are in one sub-lattice only.

In case 1, each electron in sub-lattice B has $m_B - 1$ sites blocked in B by other electrons in B and at least [at most] $m_A + 1$ [$2m_A$] sites blocked in B by electrons in sub-lattice A; one can similarly argue for the electrons in sub-lattice A. Thus in sub-lattice B(A), each electron can hop to at most $\frac{N}{2} - m_{A(B)} - m_{B(A)}$ unblocked sites and at least $\frac{N}{2} - 2m_{A(B)} - m_{B(A)} + 1$ unblocked sites.

In case 2, each electron has $m_A + m_B - 1$ sites blocked by the other electrons in the same sub-lattice. Hence, each electron has exactly $\frac{N}{2} - m_A - m_B + 1$ unblocked sites to hop to. At large repulsion, since case 2 gives electrons more number of unblocked sites to hop to, we see that the total energy is the lowest when all the electrons are present in the same sub-lattice.

As for the other extreme situation $V = 0$, for even number of electrons, the model has both sub-lattices equally occupied.

In the t_2 -V model, *the ground state energy has a slope discontinuity, with the energy increasing up to a critical value, after which it is constant for FFs $\frac{1}{4}$, $\frac{1}{3}$, and $\frac{1}{2}$ [as shown in Fig. 2 (a)].* We will now show clearly that as the interaction strength increases, *at a critical value of V/t_2 , Ising Z_2 symmetry (i.e., both sub-lattices being equally populated) is broken and only a single sub-lattice is occupied.* As depicted in Fig. 2 (b), the structure factor $S(\pi)$ jumps from zero to its maximum value [given by Eq. (16) for FFs $\frac{1}{4}$, $\frac{1}{3}$, and $\frac{1}{2}$] indicating *explosive* first-order QPT from a Luttinger liquid to a CDW.

Next, we observe that the number of electrons in even and odd sub-lattices are conserved quantities for the t_2 -V model. Therefore, GS of the system is an eigenstate of both \hat{N}_e and \hat{N}_o with eigenvalues N_e and N_o , respectively. Hence, Eq. (14) simplifies to

$$S(\pi) = \frac{4(N_e - N_o)^2}{N}. \quad (20)$$

Then, when Z_2 symmetry is respected, for even number of electrons $N_p = 2N_e = 2N_o$, we have $S(\pi) = 0$ and for odd value of N_p we have $S(\pi) = 4/N$. We find that at a critical interaction strength, as shown in Fig. 3, the following dramatic changes occur: (i) the structure factor $S(\pi)$ jumps from 0 to its maximum value $4N_p^2/N$; (ii)

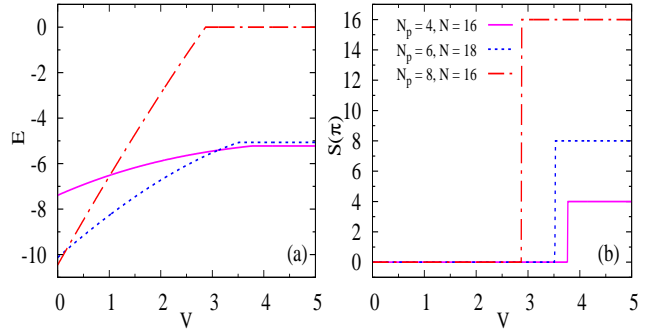


FIG. 2. (Color online) Plots, of (a) ground state energy (E) and (b) structure factor value $S(\pi)$, as a function of interaction strength (V) for the t_2 -V model in rings with N sites, N_p electrons, and hopping $t_2 = 1$.

$W(\text{odd})$ also jumps to its large V value of $-\frac{4N_p^2}{N^2}$; and (iii) $W(\text{even})$ (for $l \neq 0$) too jumps and its final value at half-filling is 1. For a fixed t_2 and N , the critical value V_C^N of V increases monotonically as N_p decreases. For $N = 16$, $N_p = 2$, and $t_2 = 1$, we get $V_C^{16} \approx 4$. From finite size scaling for half-filling, using $V_C^N - V_C^\infty \propto 1/N^2$ and system size $N \leq 20$, we obtain $V_C^\infty \approx 2.83$.

We see from the above analysis that, at a critical repulsion, the system undergoes a discontinuous transition to a *conducting commensurate CDW* state away from half-filling while at half-filling one obtains a Mott insulator. Usually commensurate CDW's are insulating (see Ref. 32) whereas our model surprisingly predicts a conducting commensurate CDW. Furthermore, quite unlike the Peierls transition, the *period of the CDW is independent of density!*

V. ANALYSIS OF THE CBM MODEL

To analyze the QPT at various FFs of a system governed by the effective polaronic Hamiltonian given in Eq. (8), we performed our calculations at values of the adiabaticity $t/\omega_0 < 1$ and $g \geq 1$ such that the small parameter $t/(g\omega_0) < 1$ and $te^{-3g^2} \ll \omega_0$. Here we report only for the conservative case $t/\omega_0 = 0.1$ since the results at other values of $t/\omega_0 < 1$ are qualitatively similar (as shown in appendix A).

As the value of g increases (in the regime of study $1 \leq g \leq 3.5$), NN and NNN hoppings compete and the system gradually transits from a large- V t-V model to a large- V t_2 -V model; thus, at values of $g \sim 1$ we expect the system to be a Luttinger liquid while at $g \sim 3$ we should get a CDW. In the next sub-sections we will demonstrate that the system indeed undergoes a Luttinger liquid to a *conducting* CDW transition with the QPT discussed in this work is quite different from the metallic Luttinger liquid to *insulating* CDW transition studied by many authors³³⁻³⁵ in a system with only NN hopping and long-

range Coulomb interaction.

A. Study of density-density correlation function, structure factor, and order parameter

First, we calculated $W(l)$ and $S(k)$ at FFs $\frac{1}{4}$ and $\frac{1}{3}$ numerically and the results are displayed in Fig. 4. Upon tuning the EPC g , the density-density correlation function $W(l)$ gradually changes its nature from decaying to oscillatory thereby exhibiting long range order; it then attains the value given by Eq. (15) at all odd values of l corresponding to the state of only one sub-lattice being occupied [see Figs. 4(a) and (c)]. Furthermore, the structure factor value $S(\pi)$ increases upon increasing g and attains the maximum value given by Eq. (16) [see Figs. 4 (b) and (d)]. These observations assert that the system undergoes QPT from a Luttinger liquid to a conducting commensurate CDW state away from half-filling with period-doubling. Thus, at a critical value of g , the Ising Z_2 symmetry (i.e., both sub-lattices being equally populated) is broken. Quite surprisingly, our model predicts a conducting commensurate CDW without an excitation gap. Furthermore, similar to the t_2 -V model, here too the period of CDW is independent of density and is, in fact, twice the lattice constant.

We will now compare $S(\pi)$ versus g behavior manifested by our model and the Holstein model in Fig. 5. We see that, while our CBM model appears to undergo a QPT, the Holstein model does not seem to do so. We ob-

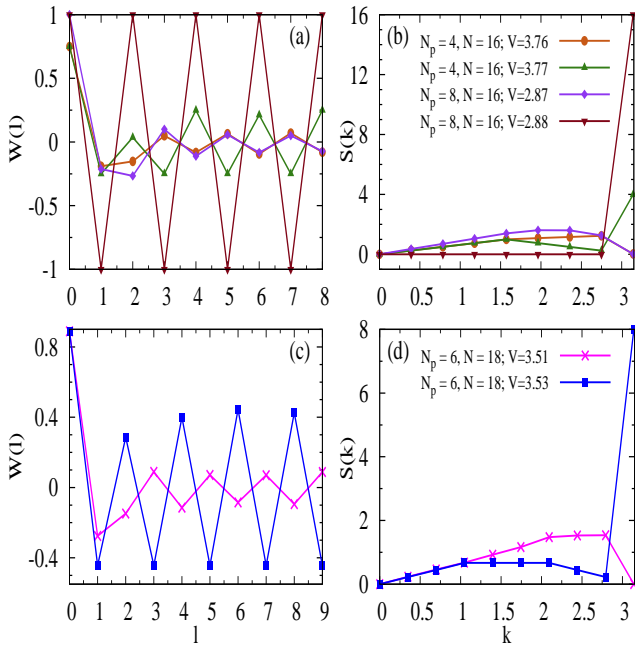


FIG. 3. (Color online) Plots of the density-density correlation function $W(l)$ and structure factor $S(k)$ for the t_2 -V model on a N -site ring with N_p electrons, interaction strength V , and hopping $t_2 = 1$. Structure factor $S(k)$ in (b) and (d) correspond to plots of $W(l)$ in (a) and (c), respectively.

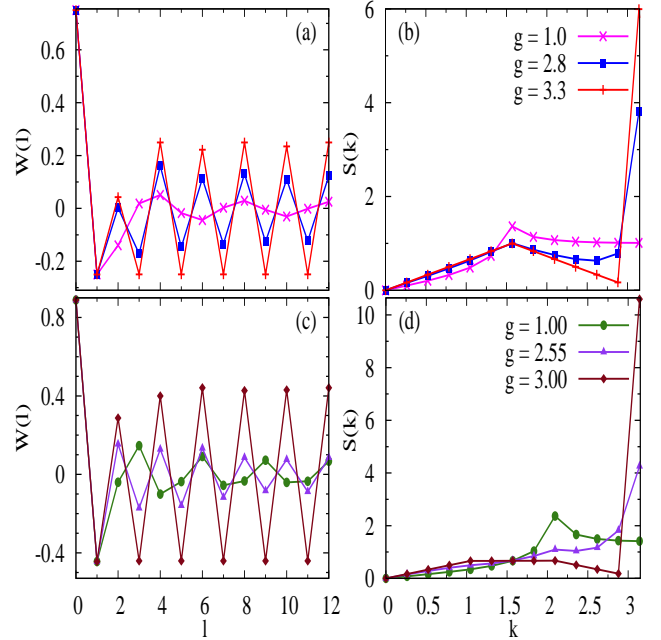


FIG. 4. (Color online) Density-density correlation function $W(l)$ in the CBM model at $\frac{t}{\omega_0} = 0.1$ and $N = 24$ for (a) $\frac{1}{4}$ -filling; and (c) $\frac{1}{3}$ -filling. Structure factor $S(k)$ at (b) $\frac{1}{4}$ -filling; and (d) $\frac{1}{3}$ -filling corresponding to plots of $W(l)$ in (a) and (c) respectively.

serve that the coefficient of NNN hopping for the Holstein model (see Eq. (9)) becomes much smaller than that of the NN hopping as EPC g increases. Hence, the Holstein model, for sufficiently larger values of g , behaves like the t -V model; whereas our model can be approximated by the t_2 -V model at large g . We know that the t -V model does not undergo a QPT away from half-filling³¹. Therefore, the Holstein model too will not undergo a QPT at a non-half FF (which is consistent with the results of Ref. 12). Thus, the Z_2 symmetry breaking QPT (at non-half filling) in our model is a unique feature which has no analog in either the Holstein model or the t -V model. Furthermore, at half-filling, the t -V model undergoes a QPT when $V = 2t^{30,31}$ while the Holstein model suffers a QPT at $g > 1^{12,19}$; on the other hand our CBM model, for the range of EPC g considered (i.e., $g \geq 1$), is always deep inside the CDW phase since the coefficient of NN repulsion is much larger than the hopping terms.

Plots of the order parameter $S^*(\pi)$ displayed in Fig. 6 also reveal signatures of QPT at FFs $\frac{1}{4}$ and $\frac{1}{3}$ and at different system sizes. Moreover, we observe that the increase in $S^*(\pi)$ becomes sharper as the system size increases. From the figures it appears that there is either a continuous or weakly first-order QPT for both the FFs.

B. Ground State Fidelity; Fidelity Susceptibility and its Scaling Behavior

Although the order parameter $S^*(\pi)$ depicts a QPT, but the nature of the transition (whether it is first-order, second-order, or KT-like) is not clear. Therefore, we take recourse to the study of the ground state fidelity (GSF) and FS to characterize the nature of the QPT. The GSF is defined as the overlap between GSs at two different but near values of the control parameter (say g and $g + \delta$) as follows:

$$F(g, \delta) = |\langle \Psi_0(g) | \Psi_0(g + \delta) \rangle|, \quad (21)$$

where $|\Psi_0\rangle$ is the GS of the system and δ is a small quantity³⁶. It is clear from Eq. (21) that $F(g, \delta)$ depends on δ . On the other hand, the FS³⁷, defined below as the second derivative of GSF³⁶,

$$\chi_F(g) \equiv \partial_\delta^2 F(g, \delta)|_{\delta=0} = 2 \lim_{\delta \rightarrow 0} \frac{1 - F(g, \delta)}{\delta^2}, \quad (22)$$

is independent of δ .

The GS of the system, after transition, becomes two-fold degenerate as either of the two sub-lattices, namely even and odd, can have the larger occupancy. Now, any linear superposition of the two degenerate states is also a GS. Therefore, the calculated GSF [i.e., the absolute value of the overlap of GS $|\Psi_0\rangle$ at two close by values of the control parameter (g and $g + \delta$)] becomes arbitrary. To eliminate arbitrariness in the estimate of GSF, we start with $\Psi_0(g)$ as our initial guess in the modified Lanczos algorithm to get the GS $\Psi_0(g + \delta)$.

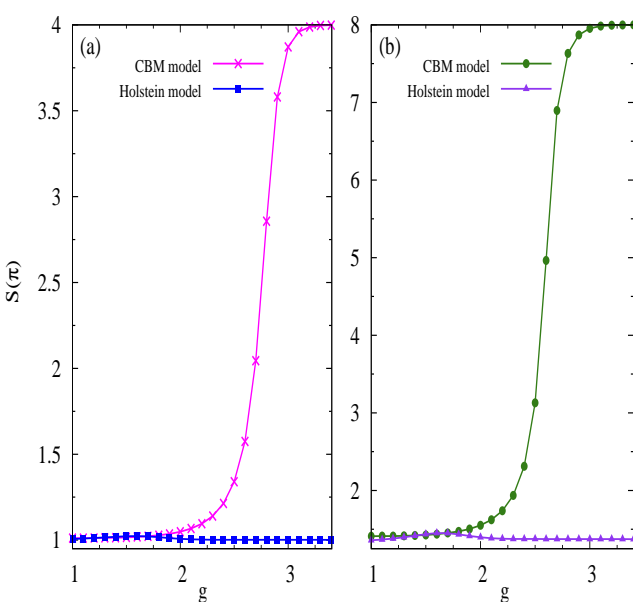


FIG. 5. (Color online) Structure factor value $S(\pi)$ at $\frac{t}{\omega_0} = 0.1$ for (a) $\frac{1}{4}$ -filling and $N = 16$; and (b) $\frac{1}{3}$ -filling and $N = 18$ in our CBM model and the Holstein model.

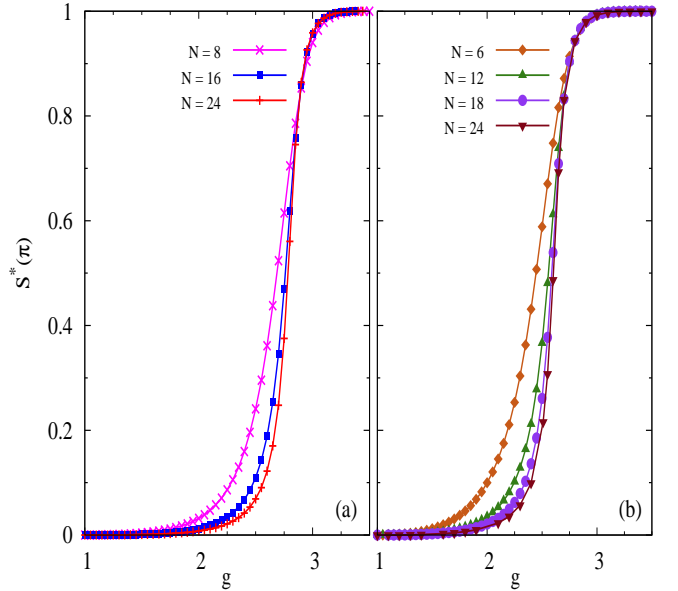


FIG. 6. (Color online) Order parameter $S^*(\pi)$ in the CBM model at $\frac{t}{\omega_0} = 0.1$ for (a) $\frac{1}{4}$ -filling; and (b) $\frac{1}{3}$ -filling.

Next, we point out a mapping that will enable us to perform fidelity calculations in systems with sizes larger than the usual sizes accessible to the modified Lanczos technique. At $\frac{N_p}{N}$ -filling in our CBM model, when NN repulsion is much larger than both the NN and the NNN hoppings, our model can be reduced to the following model at $\frac{N_p}{N-N_p}$ -filling but without NN repulsion (for similar analyses, see the treatment of the t-V model in Ref. 38 and the mapping of the t-V₁-V₂ model in Ref. 26):

$$H_{eff}^{RC} = -te^{-3g^2} \sum_j (c_j^\dagger c_{j+1} + H.c.) - \frac{t^2 e^{-2g^2}}{4g^2 \omega_0} \sum_j [c_{j-1}^\dagger (1 - n_j) c_{j+1} + H.c.]. \quad (23)$$

In the NNN hopping term, because of large NN repulsion, we have ignored the contribution of the sequential hopping depicted in Fig. 2(c) of Ref. 25. The above prescription reduces the dimension of the Hilbert space significantly from ${}^N C_{N_p}$ to ${}^{N-N_p} C_{N_p}$. From Eq. (23), we also observe that the new effective Hamiltonian contains only kinetic terms. Hence, the GS in the CDW phase has to be conducting away from half-filling.

In Fig. 7, we depict $F(g, \delta)$ and $\chi_F(g)$ as a function of g at FFs $\frac{1}{4}$ and $\frac{1}{3}$. The dip in $F(g, \delta)$ at the critical point increases with the increase in δ . This happens because of the fact that the distance between two ground states in parameter space increases with the increase in δ . However, $\chi_F(g)$ for different small values of δ coincide as $\chi_F(g)$ is independent of δ [as can be seen from Eq. (22)].

Additionally, Fig. 8 shows $F(g, \delta = 0.05)$, $\chi_F(g)$ and $\chi_{F_{max}}$ (or the peak FS) for different system sizes at FFs $\frac{1}{4}$ and $\frac{1}{3}$. The dip (peak) in $F(g, \delta)$ [$\chi_F(g)$] at the extremum

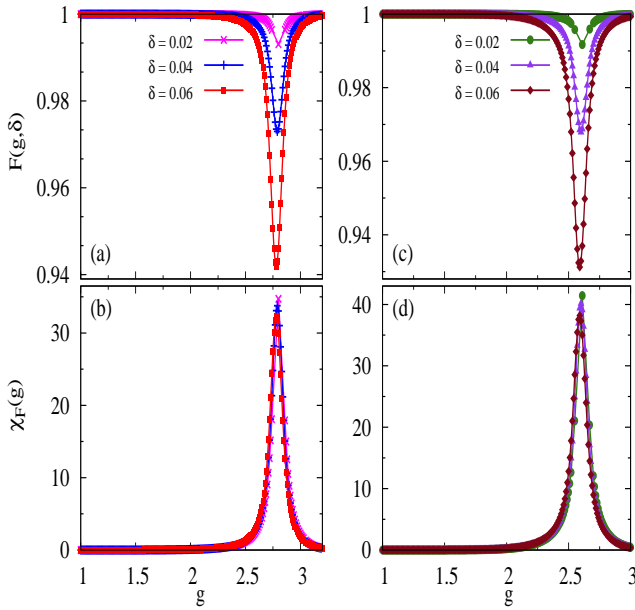


FIG. 7. (Color online) GSF $F(g, \delta)$ in the CBM model at $\frac{t}{\omega_0} = 0.1$ for (a) $\frac{1}{4}$ -filling and $N = 32$; and (c) $\frac{1}{3}$ -filling and $N = 30$. FS $\chi_F(g)$ for (b) $\frac{1}{4}$ -filling; and (d) $\frac{1}{3}$ -filling correspond to the GSF-plots in (a) and (c) respectively. For the sake of clarity, only selected points are shown for $\delta = 0.02$.

point increases with the system size N . Furthermore, for a finite system, $\chi_{F_{\max}}$ scales like^{39,40}

$$\chi_{F_{\max}} \propto N^\mu. \quad (24)$$

The logarithmic scale plot of the peak FS value $\chi_{F_{\max}}(N)$ with N shows a linear behavior (see Fig. 8(e)) which confirms a power law divergence of $\chi_{F_{\max}}(N)$ at the extremum point g_{\max} . At large N , we obtain $\chi_{F_{\max}}(N) \sim N^{2.001}$ at $\frac{1}{4}$ -filling; whereas at $\frac{1}{3}$ -filling we get $\chi_{F_{\max}}(N) \sim N^{1.868}$. The superextensive power law divergence of $\chi_{F_{\max}}$ along with the dynamical critical exponent value $z \sim 1$ rule out a KT-like transition (see appendix B for details).

In order to examine the possibility of a second-order QPT, we consider the following scaling relation^{39,40} for $\chi_F(g)$:

$$\frac{(\chi_{F_{\max}}(N) - \chi_F(g, N))}{\chi_F(g, N)} = f[N^{\frac{1}{\nu}}(g - g_{\max})], \quad (25)$$

where ν is the critical exponent of the correlation length. Interestingly, a plot of $[\chi_{F_{\max}}(N) - \chi_F(g, N)]/\chi_F(g, N)$ versus $N^{\frac{1}{\nu}}(g - g_{\max})$, as depicted in Fig. 9, shows a nice scaling relation of $\chi_F(g, N)$ with ν taking the values 1.33 ± 0.01 and 1.41 ± 0.01 for the best fits to the universal curves at FFs $\frac{1}{4}$ and $\frac{1}{3}$ respectively. The superextensive power law divergence and the scaling behavior of χ_F demonstrate that the QPT is second-order in nature.

Furthermore, as pointed out in Refs. 39 and 40, average

FS $\chi_F(g)/N$ around the critical point g_c scales like

$$\frac{\chi_F(g)}{N} \propto \frac{1}{|g_c - g|^\alpha}, \quad (26)$$

in the thermodynamic limit, with α being a critical exponent. The three exponents α , μ , and ν are related as^{39,40}

$$\alpha = \nu(\mu - 1). \quad (27)$$

The values of the critical exponent α , on using Eq. (27), turn out to be $\alpha \simeq 1.33$ and $\alpha \simeq 1.22$ for FFs $\frac{1}{4}$ and $\frac{1}{3}$ respectively. On using finite size scaling, we find the critical point g_c values to be 2.785 and 2.594 for FFs $\frac{1}{4}$ and $\frac{1}{3}$ respectively [based on positions of dips (peaks) of GSF (FS) in Fig. 8].

VI. CONCLUSIONS

We derived an effective Hamiltonian for molecular chains involving CBM at strong EPI. The spinless

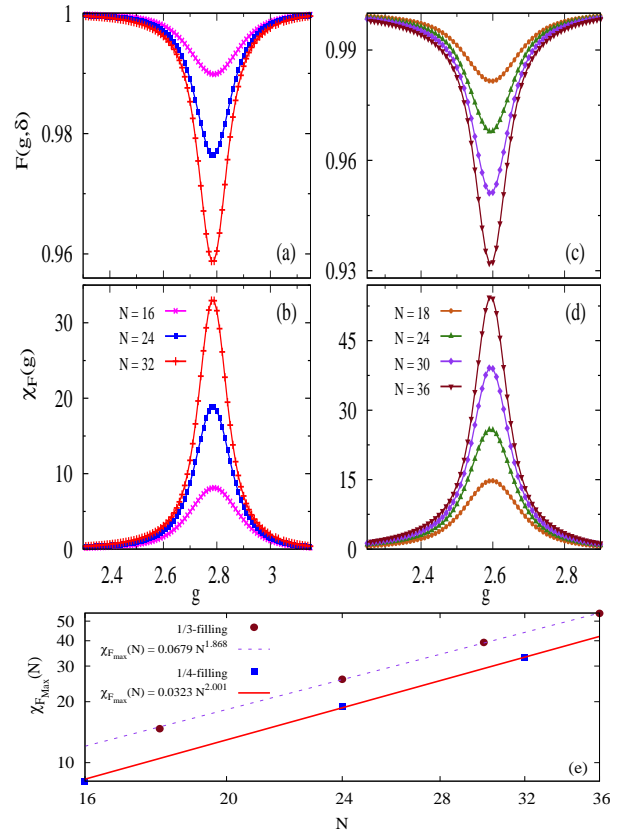


FIG. 8. (Color online) GSF $F(g, \delta)$ in the CBM model at $\frac{t}{\omega_0} = 0.1$ and $\delta = 0.05$ for (a) $\frac{1}{4}$ -filling; and (c) $\frac{1}{3}$ -filling. FS $\chi_F(g)$ for (b) $\frac{1}{4}$ -filling; and (d) $\frac{1}{3}$ -filling correspond to the GSF-plots in (a) and (c). (e) Plot of the peak values of FS $\chi_{F_{\max}}(N)$ versus N , on a logarithmic scale, at $\frac{1}{4}$ -filling and $\frac{1}{3}$ -filling and the corresponding power-law fits.

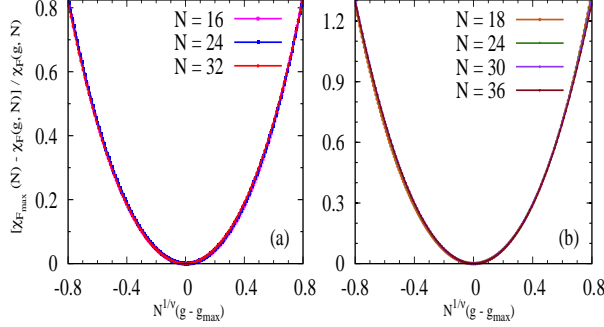


FIG. 9. (Color online) Scaling behavior of FS $\chi_F(g, N)$ in the CBM model at $\frac{t}{\omega_0} = 0.1$ for (a) $\frac{1}{4}$ -filling yielding $\nu = 1.33 \pm 0.01$ and for (b) $\frac{1}{3}$ -filling producing $\nu = 1.41 \pm 0.01$.

fermion model considered here should be relevant to perovskite systems with large onsite coulomb repulsion. Our analysis shows that our system has an effective Hamiltonian of the form

$$\begin{aligned} H_{t-t_2-V} = & -t \sum_j (c_j^\dagger c_{j+1} + \text{H.c.}) \\ & - t_2 \sum_j (c_{j-1}^\dagger (1 - 2n_j) c_{j+1} + \text{H.c.}) \\ & + V \sum_j n_j n_{j+1}, \end{aligned} \quad (28)$$

with $t_2 \ll t$ for small g (~ 1), whereas $t_2 \gg t$ for large g ($\gtrsim 3$); furthermore V is significantly larger than both t and t_2 for all values of EPC ($1 \leq g \leq 3.5$) considered. Thus, NN and NNN hoppings compete and the system transits from a large- V t-V model (with a Luttinger liquid GS) to a large- V t_2 -V model (with a period-doubling CDW GS) as g increases; our fidelity analysis shows that the QPT is second-order in nature. In the past, a density independent charge ordering has indeed been observed in manganite systems (see Fig. 2 in Ref. 41). However, since the dimensionality and number of bands are different, our findings are not directly related to these reported results. Although the reported calculations were performed for a conservative value of the adiabaticity $t/\omega_0 = 0.1$, we find that our results are qualitatively similar in the whole anti-adiabatic regime of $t/\omega_0 < 1$ (as shown in appendix A). Furthermore, we provide one more model system where the utility of GSF and FS in studying the nature of QPT is clearly demonstrated.

VII. ACKNOWLEDGMENTS

One of the authors (S. Y.) would like to thank P. B. Littlewood, S. Kos, D. E. Khmelnitskii, T. V. Ramakrishnan, Diptiman Sen, and M. Q. Lone for valuable discussions and KITP for hospitality.

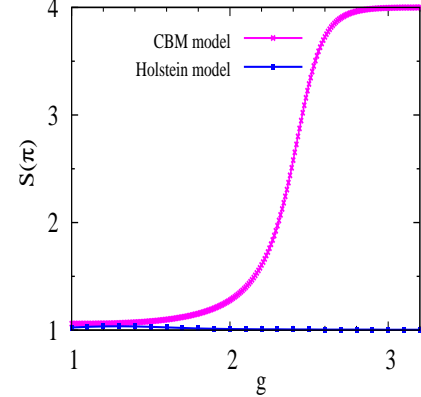


FIG. 10. (Color online) Plots of structure factor value $S(\pi)$ at $\frac{1}{4}$ -filling for $N = 16$ and $\frac{t}{\omega_0} = 0.5$.

Appendix A

In this appendix, we study our CBM model at different values of the adiabaticity parameter $\frac{t}{\omega_0}$ and for system size $N = 16$ and FF $\frac{1}{4}$. Firstly, we wish to point out that, in the entire anti-adiabatic regime, the Z_2 symmetry breaking captured by $S(\pi)$ is a novel feature of our CBM model which is not present in the Holstein model; this claim is endorsed by Figs. 5 and 10.

As depicted in Fig. 11, for various values of $\frac{t}{\omega_0}$, the order parameter $S^*(g)$ rises from 0 to 1 when the control parameter g is increased; larger values of $\frac{t}{\omega_0}$ lead to QPT occurring at smaller values of g . The GSF $F(g, \delta)$ and the corresponding FS, at different values of $\frac{t}{\omega_0}$, are portrayed in Figs. 12(a) and 12(b) respectively. The dip (peak) in the GSF (FS) occurs at smaller values of g when the adiabaticity $\frac{t}{\omega_0}$ assumes larger values.

From the above analysis, we find that our model exhibits qualitatively similar behavior for all values of the adiabaticity parameter $\frac{t}{\omega_0} \leq 1$. Furthermore, we expect

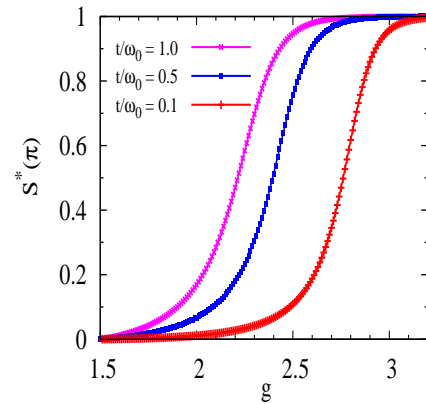


FIG. 11. (Color online) Order parameter $S^*(\pi)$ in the CBM model at $\frac{1}{4}$ -filling, $N = 16$, and for different values of $\frac{t}{\omega_0}$.

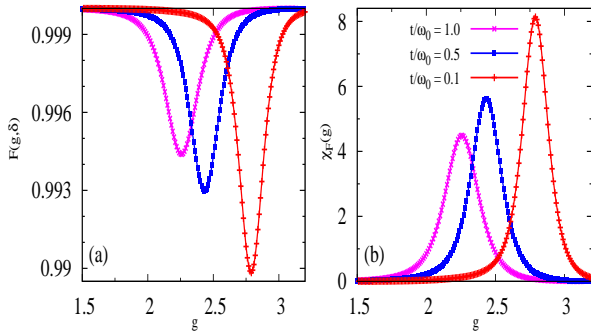


FIG. 12. (Color online) Plots of (a) GSF $F(g, \delta)$ at $\delta = 0.05$ and (b) corresponding FS in the CBM model at different values of $\frac{t}{\omega_0}$ and for $N = 16$ and $\frac{1}{4}$ -filling.

similar behavior at other FFs and system sizes as well.

Appendix B

In this appendix, we will describe a new general approach to identify a KT transition. The FS can also be written³⁷ as

$$\chi_F(g) = \sum_{n \neq 0} \frac{|\langle \Psi_n(g) | H_I | \Psi_0(g) \rangle|^2}{[E_n(g) - E_0(g)]^2}, \quad (B1)$$

where H_I is the QPT driving Hamiltonian. On the other hand, according to perturbation theory, the second order perturbation to the GS energy takes the form

$$E_0^{(2)}(g) = \sum_{n \neq 0} \frac{|\langle \Psi_n(g) | H_I | \Psi_0(g) \rangle|^2}{[E_0(g) - E_n(g)]}. \quad (B2)$$

At the KT-transition point, both the numerator and denominator of Eq. (B2) tend to zero with system size in exactly the same manner; hence no divergence results. At the extremum point, the mass gap typically vanishes with system size as

$$\Delta \equiv E_1(g_{\max}) - E_0(g_{\max}) \sim \frac{1}{N^z}, \quad (B3)$$

where z is the dynamical critical exponent. Thus, for a KT-transition the FS at the extremum point exhibits the

following behavior

$$\chi_{F_{\max}} \sim N^z. \quad (B4)$$

However, (in contrast to the KT-transition) for a first-order or a second-order transition, the numerator of Eq. (B2) (at the extremum point) does not tend to zero as fast as the denominator and hence divergence occurs in the thermodynamic limit. Therefore, the divergence in Eq. (B2) leads to an even stronger power law divergence in the FS at the extremum point (as can be seen from Eq. (B1)):

$$\chi_{F_{\max}} \sim N^\mu, \quad (B5)$$

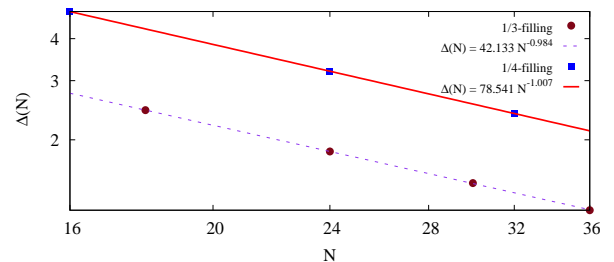


FIG. 13. (Color online) A log-log plot of the excitation energy $\Delta(N)$ versus N in the CBM model at $\frac{1}{4}$ -filling and $\frac{1}{3}$ -filling and the corresponding power-law fits.

where $\mu > z$. Now, in Fig. 13, we depict variation of the mass gap $\Delta(N)$ with N on a logarithmic scale and observe linear behavior. At large N , we obtain $\Delta(N) \sim \frac{1}{N^{1.007}}$ (i.e., $z = 1.007$) at $\frac{1}{4}$ -filling while at $\frac{1}{3}$ -filling we get $\Delta(N) \sim \frac{1}{N^{0.984}}$ (i.e., $z = 0.984$); whereas from Fig. 8(e), we find $\chi_{F_{\max}}(N) \sim N^{2.001}$ (i.e., $\mu = 2.001$) at $\frac{1}{4}$ -filling while at $\frac{1}{3}$ -filling we get $\chi_{F_{\max}}(N) \sim N^{1.868}$ (i.e., $\mu = 1.868$). Clearly, $\mu > z$ for both the FFs which rules out the possibility of a KT-transition. Hence, the QPT in our model is either first-order or second-order.

Lastly, we would like to mention that another approach, involving examining the global geometric entanglement, to detect the elusive KT quantum phase transition has been recently reported^{42,43}.

¹ A. Taraphder, R. Pandit R., H. R. Krishnamurthy, and T. V. Ramakrishnan, Int. J. Mod. Phys. B **10**, 863 (1996).

² T. Hotta, Rep. Prog. Phys. **69**, 2061 (2006).

³ J. van den Brink, and D. I. Khomskii, J. Phys.: Condens. Matter **20**, 434217 (2008).

⁴ A. Lanzara, N. L. Saini, M. Brunelli, F. Natali, A. Bianconi, P. G. Radaelli, and S. W. Cheong, Phys. Rev. Lett. **81**, 878 (1998).

⁵ D. Louca, T. Egami, E. L. Brosa, H. Röder, and A. R. Bishop, Phys. Rev. B **56**, R8475 (1997).

⁶ A. Damascelli, Z. Hussain, and Z. X. Shen, Rev. Mod. Phys. **75**, 473 (2003).

⁷ For a numerical investigation of single-polaron properties of the system in Fig. 1(b), see B. Lau, M. Berciu, and G. A. Sawatzky, Phys. Rev. B **76**, 174305 (2007).

⁸ Glen L. Goodwin and Mona Berciu, Phys. Rev. B **78**,

235120 (2008).

⁹ F. C. Zhang, and T. M. Rice, Phys. Rev. B **37**, 3759 (1988).

¹⁰ A. Szewczyk, M. Gutowska, and B. Dabrowski, Phys. Rev. B **72**, 224429 (2005).

¹¹ T. Holstein, Ann. Phys. (N.Y.) **8**, 343 (1959).

¹² S. Datta, A. Das, and S. Yarlagadda, Phys. Rev. B **71**, 235118 (2005).

¹³ See also Section V of S. Datta, and S. Yarlagadda, Phys. Rev. B **75**, 035124 (2007).

¹⁴ Martin Hohenadler, Holger Fehske, and Fakher F. Assaad Phys. Rev. B **83**, 115105 (2011).

¹⁵ J. E. Hirsch, and E. Fradkin, Phys. Rev. B **27**, 4302 (1983).

¹⁶ C. E. Creffield, G. Sangiovanni, and M. Capone, Eur. Phys. J. B **44**, 175 (2005).

¹⁷ H. Zheng, D. Feinberg, and M. Avignon, Phys. Rev. B **39**, 9405 (1989).

¹⁸ C. A. Perroni, V. Cataudella, G. De Filippis, G. Iadonisi, V. Marigliano Ramaglia, and F. Ventriglia, Phys. Rev. B **67**, 214301 (2003).

¹⁹ R. J. Bursill, R. H. McKenzie, and C. J. Hamer, Phys. Rev. Lett. **80**, 5607 (1998).

²⁰ M. Hohenadler, D. Neuber, W. von der Linden, G. Wellein, J. Loos, and H. Fehske, Phys. Rev. B **71**, 245111 (2005); M. Hohenadler, G. Wellein, A. Alvermann, and H. Fehske, Physica B **378-380**, 64 (2006).

²¹ A different type of cooperative electron-phonon interaction effect corresponding to a distance dependent electron-phonon interaction has been considered for a Fröhlich polaron by A. S. Alexandrov and P. E. Kornilovitch, Phys. Rev. Lett. **82**, 807 (1999). Interestingly, their analytic approach (like our method) is also valid for $t/\omega_0 \lesssim 1$.

²² The many-polaron problem with infinite-range electron-phonon coupling was studied for the spinless Fröhlich model by A. S. Alexandrov and P. E. Kornilovitch, J. Phys.: Condens. Matter **14**, 5337 (2002). The cooperative effect considered by these authors is long-ranged whereas our treatment of the breathing mode involves short-range EPI.

²³ For a review of many-polaron effects for both Fröhlich polarons and Holstein polarons involving spin and spinless fermions, see A. S. Alexandrov and J. T. Devreese, Advances in Polaron Physics (Springer, Berlin 2009). However, this book does not cover the dominant NNN hopping due to cooperative EPI effects considered in our paper.

²⁴ I.G. Lang, and Yu.A. Firsov, Zh. Eksp. Teor. Fiz. **43**, 1843 (1962) [Sov. Phys. JETP **16**, 1301 (1963)].

²⁵ S. Reja, S. Yarlagadda, and P. B. Littlewood, Phys. Rev. B **84**, 085127 (2011).

²⁶ S. Reja, S. Yarlagadda, and P. B. Littlewood, Phys. Rev. B **86**, 045110 (2012).

²⁷ G. V. Pai, S. R. Hassan, H. R. Krishnamurthy, and T. V. Ramakrishnan, Europhys. Lett. **64**, 696 (2003).

²⁸ A. S. Alexandrov, Europhys. Lett. **95**, 27004 (2011).

²⁹ A. Alexandrov and J. Ranninger, Phys. Rev. B **23**, 1796 (1981).

³⁰ E. R. Gagliano, E. Dagotto, A. Moreo, and F. C. Alcaraz, Phys. Rev. B **34**, 1677 (1986).

³¹ F. D. M. Haldane, Phys. Rev. Lett. **45**, 1358 (1980).

³² G. Grüner, *Density Waves in Solids*, (Addison-Wesley, Reading, MA, 1994).

³³ Sylvain Capponi, Didier Poilblanc, and Thierry Giamarchi, Phys. Rev. B **61**, 13410 (2000).

³⁴ G. Fano, F. Ortolani, A. Parola, and L. Ziosi, Phys. Rev. B **60**, 15654 (1999).

³⁵ Martin Hohenadler, Stefan Wessel, Maria Daghofer, and Fakher F. Assaad, Phys. Rev. B **85**, 195115 (2012).

³⁶ P. Zanardi, and N. Paunković, Phys. Rev. E **74**, 031123 (2006).

³⁷ W. L. You, Y. W. Li, and S. J. Gu, Phys. Rev. E **76**, 022101 (2007).

³⁸ R. G. Dias, Phys. Rev. B **62**, 7791 (2000).

³⁹ S. J. Gu, H. M. Kwok, W. Q. Ning, and H. Q. Lin, Phys. Rev. B **77**, 245109 (2008); *ibid.* **83**, 159905(E) (2011).

⁴⁰ S. J. Gu, Int. J. Mod. Phys. B **24**, 4371 (2010).

⁴¹ G. C. Milward, M. J. Calderon, and P. B. Littlewood, Nature **433**, 607 (2005).

⁴² Román Orús and Tzu-Chieh Wei, Phys. Rev. B **82**, 155120 (2010).

⁴³ Jean-Marie Stéphan, Grégoire Misguich, and Fabien Alet, Phys. Rev. B **82**, 180406 (2010).